

RESEARCH ARTICLE

Linewidth narrowing in free-space-running diamond Brillouin lasers

Duo Jin^{1,2,†}, Zhenxu Bai^{1,2,3,†}, Zhongan Zhao^{1,2}, Yifu Chen^{1,2}, Wenqiang Fan^{1,2}, Yulei Wang^{1,2}, Richard P. Mildren³, and Zhiwei Lü^{1,2}

¹Center for Advanced Laser Technology, Hebei University of Technology, Tianjin, China

²Hebei Key Laboratory of Advanced Laser Technology and Equipment, Tianjin, China

³MQ Photonics Research Centre, Department of Physics and Astronomy, Macquarie University, Sydney, Australia

(Received 28 March 2023; revised 20 May 2023; accepted 30 May 2023)

Abstract

This study analyzes the linewidth narrowing characteristics of free-space-running Brillouin lasers and investigates the approaches to achieve linewidth compression and power enhancement simultaneously. The results show that the Stokes linewidth behavior in a free-space-running Brillouin laser cavity is determined by the phase diffusion of the pump and the technical noise of the system. Experimentally, a Stokes light output with a power of 22.5 W and a linewidth of 3.2 kHz was obtained at a coupling mirror reflectivity of 96%, which is nearly 2.5 times compressed compared with the linewidth of the pump (7.36 kHz). In addition, the theoretical analysis shows that at a pump power of 60 W and a coupling mirror reflectivity of 96%, a Stokes output with a linewidth of 1.6 kHz and up to 80% optical conversion efficiency can be achieved by reducing the insertion loss of the intracavity. This study provides a promising technical route to achieve high-power ultra-narrow linewidth special wavelength laser radiations.

Keywords: high power; narrow linewidth; single-frequency laser; stimulated Brillouin scattering

1. Introduction

High-power narrow linewidth single-frequency lasers have attracted extensive interest due to their superior characteristics in some fields, such as gravitational wave detection^[1], quantum information optics^[2], atomic physics^[3] and nonlinear frequency conversion^[4–6]. The most widely used approaches to obtain high-power narrow linewidth lasers are master oscillator power amplification (MOPA) structures based on low-power narrow linewidth seeds^[7,8] and single-cavity structures with direct high-power output^[9,10]. However, in MOPA systems, aside from the problems of beam quality deterioration and mode instability due to thermal accumulation^[11], the linewidth broadening introduced by spontaneous radiation during the amplification process cannot be ignored. Using a single cavity to obtain a high-power single-frequency laser overcomes the complexity of laser structures but faces the problem that the linewidth cannot be further narrowed due to strong pumping intensity noise^[9]. In addition, the output wavelength in the above-

mentioned solutions is critically dependent on the energy level structure of the gain medium, which limits the applicability of conventional high-power single-frequency lasers in some special wavelength laser applications (e.g., sodium-guided star research)^[12]. The emergence of optical nonlinear frequency conversion techniques accompanies the development of high-power laser technology to provide a new perspective for achieving high-power narrow linewidth laser radiation at specific wavelengths. Of these, stimulated Brillouin scattering (SBS), a third-order nonlinear effect, offers excellent advantages in applications of realizing ultra-narrow linewidth lasers^[13–15], microwave photonics^[16–18] and optical storage^[19]. The heavy attenuation mechanism of acoustic phonons combined with the strong feedback provided by the cavity enables micro-waveguide Brillouin lasers (BLs) to produce laser outputs far below the linewidth of conventional single-frequency lasers and close to the quantum noise limit^[20,21]. Similarly, strong linewidth narrowing has been reported in fiber BLs^[22] and laser outputs of sub-kHz magnitude subject to technical noise^[23]. These demonstrations based on waveguide structures also face some insurmountable problems in power boosting. The high Q cavity achieves a narrow linewidth with a concomitant lowering of the threshold of the higher-order Stokes frequency component, resulting in a limited single-frequency BL power scale^[24].

Correspondence to: Zhenxu Bai, Yulei Wang and Zhiwei Lü, Center for Advanced Laser Technology, Hebei University of Technology, Tianjin 300401, China. Email: baizhenxu@hotmail.com (Z. Bai); wyl@hebut.edu.cn (Y. Wang); zhiweilv@hebut.edu.cn (Z. Lü)

[†]These authors contributed equally to this work.

The phase-matching condition of high-order Stokes light can be broken using inter-mode scattering through a tailored cavity structure^[25], but the thermal effects accumulated in the cavity at power scaling detune the phase-matching condition of the single-frequency BL, leading to power-clamping phenomena^[20]. The mechanism of Stokes linewidth compression in fiber BLs relies on the employment of long fiber cavities^[26], whereas their phase-matching conditions require a free spectral range (FSR) comparable to the Brillouin gain linewidth, which thereby limits further linewidth compression and power boosting. Increasing the pump power in anticipation of achieving a single-frequency power increase will inevitably produce spontaneous radiation of higher-order Stokes frequency components^[22,27].

Addressing the power improvement constraint faced by waveguide BLs, free-space-running BLs offer a solution to achieve high power and narrow linewidth output. Separating the cavity and gaining medium in the spatial cavity facilitates thermal management and control of phase-matching conditions at high power. In addition, the diversity of Brillouin gain materials makes it possible to realize high-power lasers with narrow linewidths at special wavelengths. The power of the free-space-running BL was increased from the initial 20 mW restricted by the gain level^[28] to a level exceeding 20 W without saturation of the power curve^[29]. The output wavelength also extends from the visible to the near-infrared band^[28–30]. However, even with these impressive demonstrations, the characteristics of Stokes linewidth narrowing in spatially structured BLs have not been reported so far, which has been the most crucial basis for extensive research and development of BLs. In our previous study, we reported that the single-frequency BL output at 1064 nm and 46.9 kHz exhibited severe broadening compared with the linewidth of the pump (~7 kHz), which was attributed to the effect of technical noise at that time^[29].

This study theoretically and experimentally analyzes the linewidth narrowing characteristics of free-space-running BLs. Targeting ultra-narrow laser linewidth measurements, we analyzed the influence of fiber length on linewidth measurement results from the mechanism of delayed self-heterodyne interferometry. Subsequently, the corresponding structures are used for BL linewidth measurements at different coupling rates. Based on the analysis of the experimental results, we discuss a solution for simultaneous power enhancement and linewidth compression in spatially structured BLs.

2. Experiments and results

The operation mechanism and structure of the BL and the linewidth measurement system are shown in Figure 1. The gain medium used in the experiments was a Brewster-cut diamond (4 mm × 1.2 mm × 5 mm, Element Six) with polarization parallel to <001>, which is consistent with the

direction of maximum Brillouin gain through the crystal. In addition, the diamond was mounted on top of a copper heat sink that was actively temperature controlled to 20°C by a thermoelectric controller, as shown in Figure 1(b). The pump laser had a maximum power of 60 W that was emitted from a fiber-based optical amplifier (OA) and used a single-frequency seed laser (seed) with a linewidth of less than 10 kHz at 1064 nm. The Brillouin cavity was a ring cavity with a free spectral range (FSR) of approximately 560 MHz. The pump beam was injected into the fundamental mode of the Brillouin cavity using focusing lenses (f1 and f2) and reflectors (HR1 and HR2). In addition, the cavity length was adjusted to support the dual resonance of the pump and Stokes field frequencies^[29]. Frequency locking of the pump field to the cavity was achieved using the Pound–Drever–Hall frequency stabilization technique^[31]. The generated Stokes field was emitted in the opposite direction of the incident pump beam when the pump field intensity exceeded the Stokes threshold and then separated from the system using an isolator (ISO).

The two sets of critical parameters in the resonant cavity are the intrinsic loss rate (γ_{in}) and external coupling rate (γ_{ex}) as well as the intrinsic Q value ($Q_{in} = \omega/\gamma_{in}$) and load Q value ($Q_L = \omega/\gamma = \omega/(\gamma_{in} + \gamma_{ex})$), where Q_L is the total Q value of the system^[32,33]. The intrinsic loss and external coupling loss in the spatial cavity can be expressed as $\gamma_{in} = L_0 \times \text{FSR}$ and $\gamma_{ex} = -\ln R_1 \times \text{FSR}$, respectively^[34]. L_0 is the passive loss caused by the rest of the optical elements in the cavity except for the coupling mirror, and R_1 is the reflectivity of the coupling mirror. The fundamental linewidth of a resonant pumped BL can be expressed as follows^[35,36]:

$$\Delta\nu_S = (1 + \alpha^2) \left(\frac{\Gamma}{\gamma + \Gamma} \right)^2 \frac{\hbar\omega_S^3 n_{th}}{4\pi Q_L Q_{ex} P_{Sout}} + \left(\frac{\gamma}{\gamma + \Gamma} \right)^2 \Delta\nu_P. \quad (1)$$

The first part of the equation indicates the linewidth caused by the thermal phonon noise^[37,38], and the second term indicates the Stokes linewidth caused by the pump phase diffusion^[26]. Here, α is the linewidth broadening factor (zero when the Stokes frequency is not detuned), Q_{ex} is the Q value that describes the coupling loss, \hbar is the reduced Planck constant, $\Gamma = 2\pi \Delta\Omega_B$ is the Brillouin gain linewidth, $n_{th} \approx k_B T / \hbar\Omega_B$ is the thermal quantum number of the acoustic mode, $\Delta\nu_P$ is the pump linewidth and P_{Sout} is the output power of Stokes. It can be found that the Stokes linewidth of the BL is determined by the properties of the gain medium and the cavity parameters. Among these parameters, the coupling mirror reflectivity influences the Stokes output power and efficiency and determines the Stokes output linewidth. Here we choose three different sets of coupling mirror reflectance for the experiment: $R_1 = 96\%$, $R_1 = 97\%$ and $R_1 = 98.5\%$. The passive loss L_0 of the Brillouin cavity in Figure 1(b) is about 0.015, corresponding to a Q_{in} of

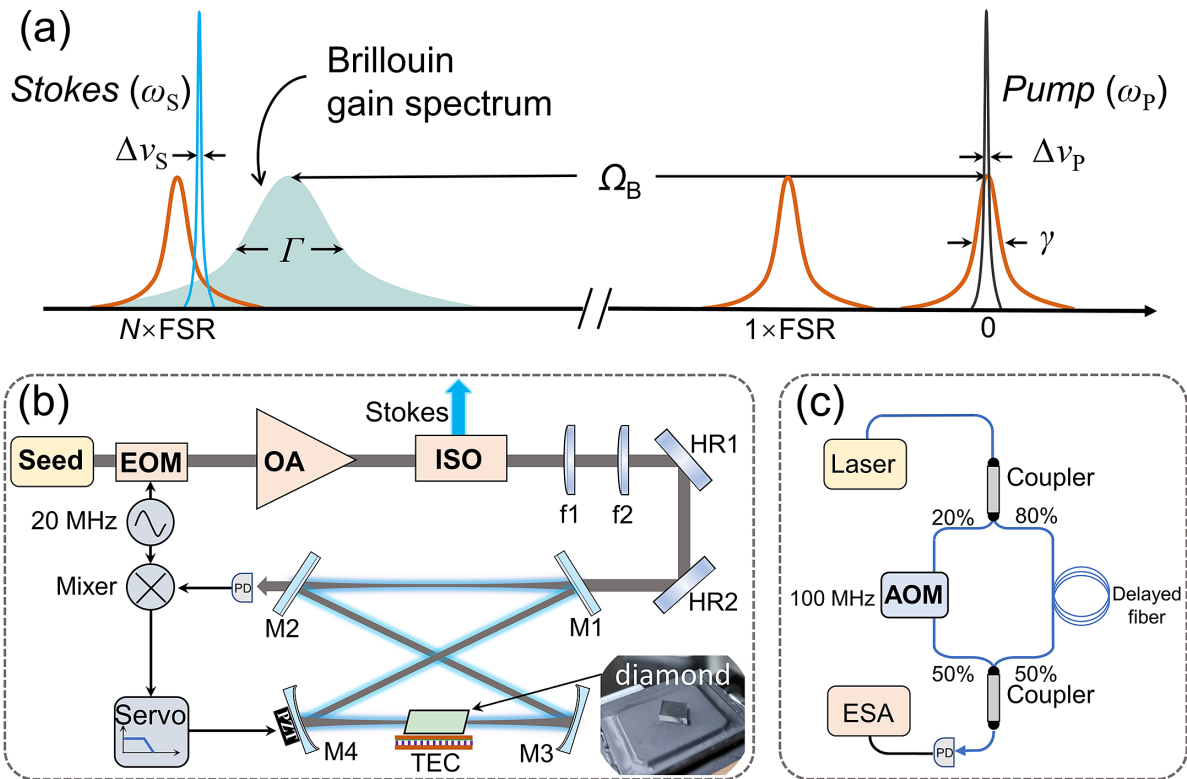


Figure 1. Illustration of the phase match, experimental setup and linewidth measurement system of a free-space, free-running BL based on a diamond. (a) Demonstration of the Brillouin gain process. The grey curve refers to the cavity resonant mode with full width at half maximum (FWHM) γ . The red (blue) curves refer to pump (Stokes) frequency ω_p (ω_s) with the linewidth of $\Delta\nu_p$ ($\Delta\nu_s$). The Brillouin gain spectrum linewidth (Γ) and frequency shift (Ω_B) are also indicated. (b) Schematic layout of a free-space, free-running BL based on a diamond (EOM, electronic optical modulator; OA, optical amplifier; ISO, isolator; f1 and f2, lenses; HR1 and HR2, high reflection mirrors; M1, coupler mirror; M2, high reflectivity plane mirror; M3 and M4, high reflectivity concave mirrors; PD, photodetector). (c) Linewidth measurement schematic. The beam is divided into two components using a 20%/80% coupler. The first component passes through an acoustic optical modulator (AOM) to generate a frequency shift of 100 MHz, and the second is delayed using a delay line (Nufern, 1060-XP). The beat note with a center frequency of 100 MHz is generated in the PD after the two components are recombined using a 3 dB coupler and analyzed by an electric spectrum analyzer (ESA) (RSA5032, Rigol).

Table 1. Stokes linewidths corresponding to different coupling mirror reflectivities.

R_1	$\gamma_{ex}/2\pi$ (MHz)	$\gamma/2\pi$ (MHz)	Q_{ex} ($\times 10^8$)	Q_L ($\times 10^8$)	$\Delta\nu_{S,T}$ (Hz)	$\Delta\nu_{S,P}$ (kHz)
96%	3.64	4.97	0.77	0.56	2.12×10^{-5}	1.73
97%	2.71	4.05	1.04	0.69	1.56×10^{-5}	1.38
98.5%	1.34	2.68	2.09	1.05	7×10^{-6}	0.83

2.1×10^8 . Assuming that there is no frequency detuning of the Stokes output ($\alpha = 0$), the linewidth due to thermal phonon noise (denoted as $\Delta\nu_{S,T}$) and the linewidth due to phase diffusion of the pump (denoted as $\Delta\nu_{S,P}$) are calculated using these parameters for the Stokes output at three sets of coupled mirror reflectivities, as shown in Table 1.

The resonant width γ , determined by the coupler reflectivity and inherent loss of the cavity, is of the same order of magnitude as the Brillouin gain width Γ ($2\pi \times 5.3$ MHz) of the diamond at 1064 nm^[29]. Therefore, the current system does not satisfy the adiabatic approximation ($\gamma \ll \Gamma$), that is, the Stokes linewidth behavior is dominated by the phase diffusion of the pump, which is similar to the linewidth behavior of most single-pass pumped fiber BLs^[22,26]. Consequently, the linewidth at the kHz level is much smaller than that of most conventional inversion lasers. Precisely

measuring the Stokes linewidth experimentally is considerably significant for the study of BLs. Here we have adopted a short fiber delay method based on a delayed self-heterodyne structure to determine the linewidth of Stokes output, which is given in Figure 1(c). The photocurrent spectral density (PSD) function of the photodetector output after the laser passes through the measurement structure is expressed as follows^[39,40]:

$$S = S_1 \times S_2 + S_3; \tag{2a}$$

$$S_1 = \frac{P_0^2}{4\pi} \frac{\Delta f}{\Delta f^2 + (f - f_1)^2}; \tag{2b}$$

$$S_2 = 1 - \exp(-2\pi \tau_d \Delta f) \left(\cos(2\pi \tau_d (f - f_1)) + \Delta f \frac{\sin 2\pi \tau_d (f - f_1)}{f - f_1} \right); \tag{2c}$$

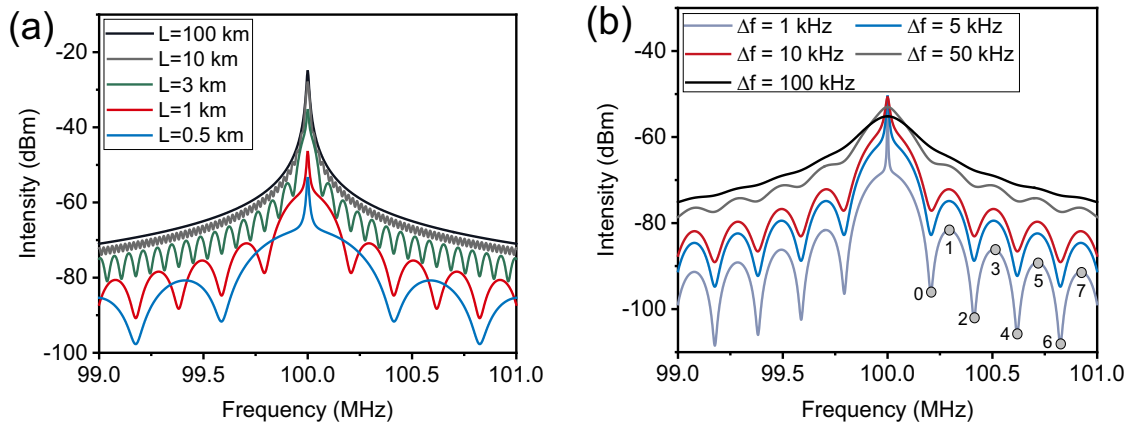


Figure 2. (a) PSD at different fiber lengths for a linewidth of 1 kHz. (b) PSD spectrum at different laser linewidth values for a fiber length of 1 km.

$$S_3 = \frac{\pi P_0^2}{2} \exp(-2\pi \tau_d \Delta f) \delta(f - f_1). \quad (2d)$$

Here, S_1 is the Lorentz function, whose spectral profile is unaffected by the fiber length, S_2 is the period modulation function, S_3 is the δ function, Δf is the linewidth, and P_0 and τ_d relate to the beat frequency signal power and delay time, respectively.

Figure 2 shows the PSD for different lengths of the delayed fiber for a laser linewidth of 1 kHz and the variation of the PSD with different linewidth values for a fiber length of 1 km. From Figure 2(a), the longer the fiber length, the smaller the amplitude and period of the function (the closer the first minima to the center frequency). When the fiber length increases to a certain degree, $S_2 \approx 1$, the modulation of the PSD profile can be neglected, and the PSD shows a Lorentzian lineshape. The traditional delayed self-heterodyne linewidth measurement scheme uses that Lorentz spectrum. However, the traditional method of sampling Lorentzian spectral lines has some limitations. For example, when the laser linewidth is extremely narrow, the delayed fiber can reach hundreds to thousands of kilometers, and such a fiber length introduces additional $1/f$ noise that makes the measurement results unreliable^[39,41]. However, it can also be found in Figure 2(b) that the depth of the interferometric envelope is definitely related to the laser linewidth as the modulation period of the spectral lines introduced by S_2 is a definite value, and the narrower the linewidth, the more distinct the envelope depth of the PSD.

Therefore, the curve of PSD as a function of linewidth can be obtained under the determination of the fiber length and acoustic optical frequency shifter. Considering that the extreme points close to the central frequency are less sensitive to the electric spectrum analyzer (ESA) noise floor^[35], the difference between the vertical axis values at the two successive extreme points $m = 0$ and $m = 1$ on the right-hand side of the PSD is taken here (see Figure 2(b)), and the relationship between the line width and the difference in

magnitude is obtained as follows^[41]:

$$\begin{aligned} \Delta S(\Delta f) &= S(m=1) - S(m=0) \\ &= 10 \log_{10} \frac{(\Delta f^2 + (\frac{c}{2nL})^2) (1 + \exp(-\frac{2\pi nL}{c} \Delta f))}{(\Delta f^2 + (\frac{3c}{2nL})^2) (1 - \exp(-\frac{2\pi nL}{c} \Delta f))}. \end{aligned} \quad (3)$$

Once ΔS is determined, the linewidth of the laser to be measured can be obtained by numerically solving Equation (3). In the experiments, subject to the influence of the instrument noise floor and $1/f$ noise introduced by long fibers, there should be an optimal value for the length of the fiber, that is, satisfying the extreme point near the center frequency and the envelope amplitude with significant contrast. The BL system with a high-power pumping source is seeded by a narrow linewidth semiconductor laser with a linewidth of 5.1 kHz using frequency noise integration. We use this laser as a light source to explore the optimal value of fiber length for the linewidth measurement system. The frequency offset $f(m=1)$ from the center of the first extreme point ($m=1$) on the right-hand side for different delay fiber lengths and the absolute value ΔS^* of the difference in envelope amplitude corresponding to a laser linewidth of 5 kHz are given in Figure 3. From Figure 3(a), as the fiber length increases, ΔS^* and $f(m=1)$ gradually decrease and tend to zero. After the fiber length exceeds the position where $f(m=1) = 0$ (point 1), the PSD enters the transition region from the envelope spectrum to the Lorentz spectrum. The PSD in this region exhibits a weakly modulated Lorentzian type with $S(m=1) < S(m=0)$. When the fiber length increases until the weak modulation disappears (point 3, $l = c \times 6\tau_c = 600$ km; τ_c represents the laser coherence time), the PSD shows a Lorentzian pattern at this point. For comparison purposes, the coherence length corresponding to the laser linewidth is also indicated in Figure 3(a) (point 2, $l = c \times \tau_c = 100$ km). The result shows that the Lorentz spectrum method requires the use of a delay much larger than the coherence time ($\tau_d > 6\tau_c$) to eliminate the influence of the interference envelope, while the introduction of long

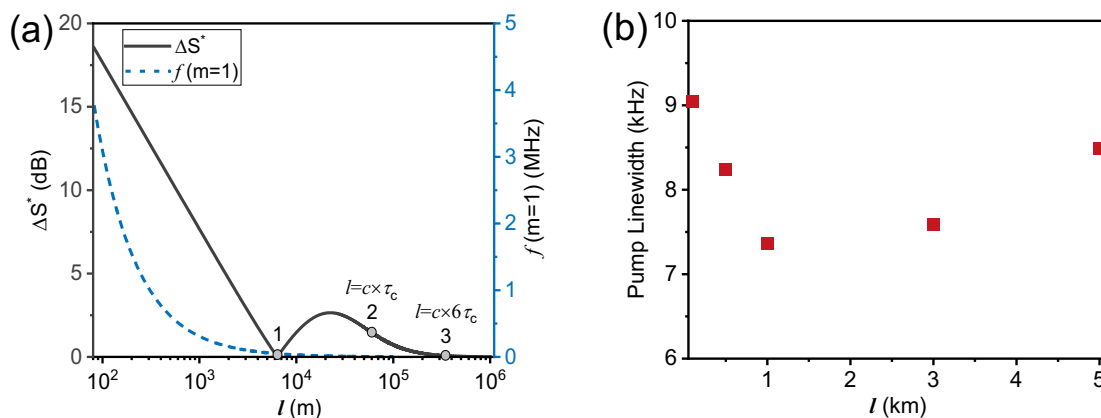


Figure 3. (a) Amplitude of the envelope differences and the frequency shift of the first extreme value point ($m = 1$) compared with the center at different fiber lengths for a linewidth of 5 kHz. (b) Experimentally measured linewidth values for a semiconductor laser corresponding to different fiber lengths.

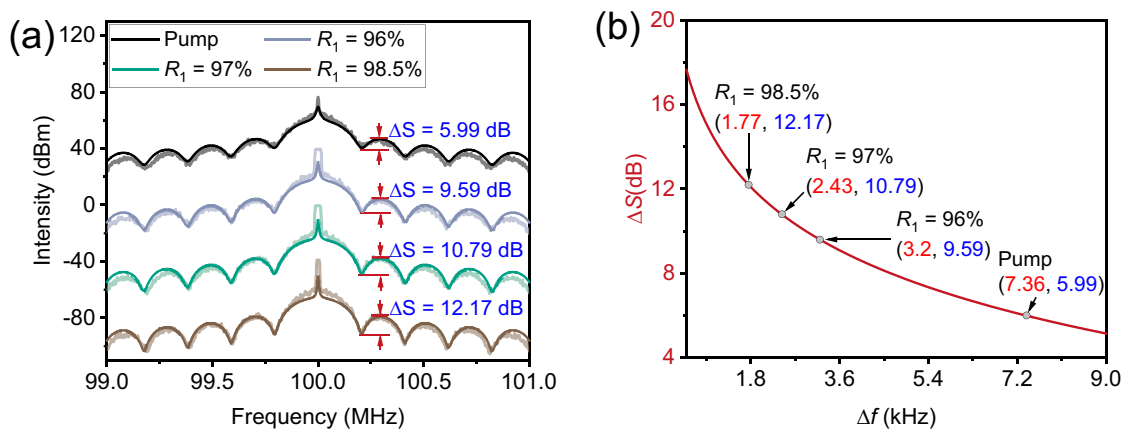


Figure 4. Stokes linewidth corresponding to the reflectivity of the three sets of coupling mirrors at 60 W power pumping. (a) Power spectrum of the corresponding delayed self-heterodyne amplitude difference. (b) Linewidth and envelope amplitude difference curves calculated by the coherent envelope method.

fibers will inevitably introduce noise into the laser to be measured, making the measurement results unreliable^[42]. Linewidth measurement using the envelope becomes a new method to solve the linewidth calibration of ultra-narrow linewidth lasers.

We experimentally measured the linewidth of the laser mentioned above by selecting five delay lengths from the envelope region (left-hand side of point 1) in Figure 3(a) to determine the optimal fiber length for the measurement system, and the results are shown in Figure 3(b). It can be seen that the difference in the results for different delay fiber lengths within the selected envelope is more than 1 kHz. In particular, the linewidth values obtained using 100 m delay fiber measurements reached 9 kHz. The corresponding extreme points at this delayed fiber length are far from the center frequency. This results in the PSD being disturbed by the ESA noise floor and the amplitude difference being less than the ideal level, resulting in a larger calculated linewidth value. When the delayed fiber is 3 km and above, the amplitude and period of the envelope start to become insignificant,

considering the presence of inevitable $1/f$ noise, which is measured to be approximately 8.6 kHz. For the laser to be measured, the PSD at 1 km delay is independent of the noise floor and free of $1/f$ type frequency noise, with a distinct envelope and significant amplitude difference. The result is closer to the actual level, with a corresponding linewidth of 7.36 kHz. The laser linewidth measured here is greater than the integral linewidth because the integral linewidth is linearly fitted to the frequency noise within the β split line and subsequently integrated, which will inevitably ignore part of the frequency noise, resulting in the corresponding integral linewidth narrowing^[43]. The BL experiments were conducted according to the three sets of coupling mirror reflectivities selected earlier, and the Stokes linewidth was measured using a delayed fiber of 1 km at maximum pump power operation. The results obtained are shown in Figure 4.

As the reflectivity of the coupling mirror increases, the Stokes output linewidth gradually narrows. The Stokes linewidths corresponding to the three sets of coupled mirror reflectivities are 3.2, 2.43 and 1.77 kHz, respectively, which

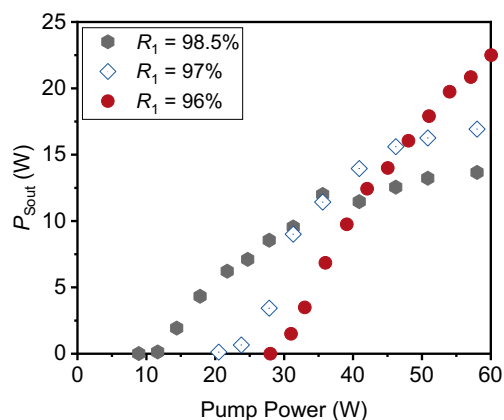


Figure 5. Stokes power with different coupling mirror reflectivities.

achieve linewidth compression compared with the pump. Even at 96% reflectivity of the coupling mirror, the linewidth is still compressed by a factor of nearly 2.5. This result is much smaller than the previously reported Stokes linewidth of 46.9 kHz measured with the same parameters^[29] because the delayed fiber used for the linewidth measurements in the previous experiments was 100 m, which caused the envelope frequency deviation to be too large, causing a portion of the corresponding PSD to be swamped with instrumental noise and leading to large calculated results.

The experimental results presented here illustrate that increasing the coupling mirror reflectivity reduces the Stokes linewidth. It can also be seen that the corresponding linewidth compression trend is consistent with that predicted in Table 1, but the linewidth results are all higher than the theoretically calculated values. We attribute the difference between the experimental measurements and the theoretical values to the introduction of additional technical noise^[26] (e.g., ambient noise and electronic noise of the locking system).

The pump–Stokes power curves corresponding to the three reflectivities are given in Figure 5. The increase in the coupling rate contributes to the lowering of the threshold. The threshold value is about 29 W at a coupling rate of 96% and decreases to 8.9 W when the coupling rate increases to 98.5%. The increased coupling rate decreases the Stokes output power and efficiency at high-power pumping. At the maximum pumping power, the Stokes output powers corresponding to the three sets of reflectivities are 22.5, 16.9 and 13.6 W, and the corresponding optical conversion efficiencies are 37.5%, 29.1% and 23.4%, respectively.

3. Discussion

Table 2 gives the system parameters and corresponding output results for the waveguide, fiber and space-structured BLs. The waveguide structure results in a much smaller overall level of corresponding Stokes linewidth than the

other two structures due to the low intrinsic and coupling losses combined with the wider Brillouin gain linewidth. It is worth noting, however, that the corresponding output power is limited to the milliwatt order due to the smaller coupling loss and size. The linewidth narrowing mechanism in optical fibers relies on the use of long fiber cavities. While the use of large mode field fibers boosts the corresponding power, further realization of power enhancement and linewidth compression is limited by the higher-order Stokes frequency components generated. The higher Stokes gain level in spatially structured BLs is determined by the high pump power, thus allowing higher conversion efficiency at higher power levels.

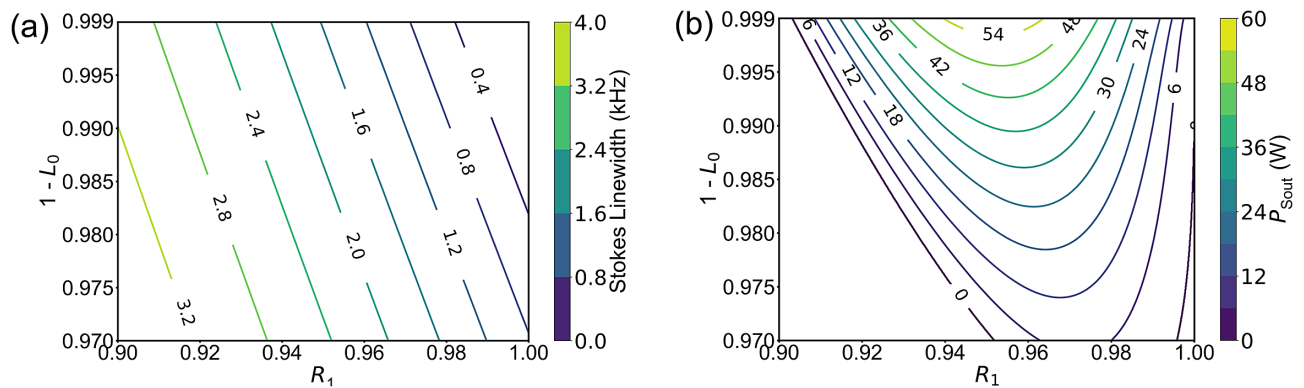
Since free-space-running BLs are designed for high power and narrow linewidth, the phase diffusion model for Stokes linewidths and the previously reported power model^[48] are used here to analyze the influence of intrinsic and coupling losses on the Stokes output linewidth and power. Taking the variation of the passive loss L_0 in the cavity from 0.001 to 0.03 and the coupling mirror reflectivity R_1 from 0.9 to 0.9999, the variation of the Stokes linewidth and power at a fixed pump of 60 W is plotted as shown in Figure 6.

With the pass loss determined, the linewidth compression effect becomes significant as the reflectivity of the coupling mirror increases. Since the passive loss is negligible compared with the coupling loss, further compression of the Stokes linewidth by reducing the passive loss is ineffective. It is worth noting that although this term does not affect the linewidth behavior, the smaller the passive loss, the higher the pumping enhancement in the cavity and the Stokes output power. Reducing the passive loss helps to improve the linewidth compression effect and conversion efficiency of the Stokes output. In the BL system mentioned in this paper, the passive losses in the cavity are primarily due to the introduction of the Brewster element. By replacing the flat-cut medium, the corresponding loss can be reduced from 0.015 to 0.005. Although the linewidth is only reduced by almost 200 Hz to approximately 1.3 kHz, the corresponding power is increased by 20 W to almost 48 W, where the optical conversion efficiency reaches 80%.

In addition to the two parameters mentioned above, the gain bandwidth of the Brillouin medium also affects the compression of the Stokes linewidth. For example, when the gain linewidth is increased from 5 to 40 MHz, the Stokes linewidth decreases from 1.7 kHz to 90 Hz. However, as can be seen from the previous experimental results, the broadening introduced by the technical noise is not negligible when the Stokes linewidth is reduced to a certain level. The linewidth of the BL system is mainly determined by the technical noise (e.g., environmental vibration, circuit locking noise) when the Stokes optical fundamental linewidth determined by the system parameters is much smaller than the broadening caused by the system technical noise. Further narrowing of the Stokes linewidth

Table 2. Platform parameters and corresponding output linewidth and power in several BLs.

Platform	Materials	λ (nm)	$\gamma/2\pi$ (MHz)	FSR (GHz)	Γ_B (MHz)	Output parameters	
						Linewidth (Hz)	Power (W)
Waveguides	CaF ₂ ^[36]	1064	0.44	~11	12.2	0.3×10^{-3}	10^{-6}
	Silica ^[37,38]	1545	1	11	51	~6	35×10^{-6}
	Silicon ^[25]	1535	13	1.57	13.1	13×10^3	0.17×10^{-3}
	Si ₃ N ₄ -based SiO ₂ ^[24]	674	16.1	3.587	290	269.7	9×10^{-3}
	As ₂ S ₃ ^[44,45]	1548		1.58	34	100×10^3	5×10^{-3}
Fiber	Ge-doped ^[27]	1064	4.98	13×10^{-3}	16	170×10^3	4.9
	As ₂ S ₃ ^[46]	1952	23	26×10^{-3}	21.5	8×10^3	1.08
	Silica ^[47]	1550	2.2	$\sim 10 \times 10^{-3}$	20	2.4×10^3	0.1
Free space	Fused silica ^[28]	732	0.025	120	100	<500	25×10^{-3}
	Diamond (this work)	1064	4.97	~0.56	5.3	3.2×10^3	22.5

**Figure 6.** (a) Stokes output linewidth determined by passive loss and coupling mirror reflectivity. (b) Stokes output power determined by passive loss and coupling mirror reflectivity at a fixed pump power of 60 W.

requires the suppression of technical noise from technical aspects, such as frequency stabilization^[32,49]. Overall, it is apparent from the above study that using free-space-running BLs can achieve narrower laser radiation compared with a pump. Combined with the inherent low quantum loss of the SBS process, it is expected that ultra-narrow linewidth laser radiation close to the quantum conversion limit can be achieved.

4. Conclusion

This study theoretically and experimentally analyzed the linewidth narrowing characteristics of free-space-running BLs and analyzed the methods to simultaneously achieve linewidth compression and power enhancement. Experimental results show that the Stokes linewidth behavior in free-space-running Brillouin cavities is determined by a combination of phase diffusion of the pump light and technical noise. At a coupling mirror reflectivity of 96%, we obtained a Stokes output with a power of 22.5 W and a linewidth of 3.2 kHz, which is nearly 2.5 times compressed compared with the linewidth of the pump. In addition, a Stokes light output of 1.7 kHz and 13.6 W was achieved by increasing the coupling mirror reflectivity to 98.5%. Furthermore, we analyzed the solution of simultaneously improving the output efficiency and linewidth compression by replacing

the Brewster element with a parallel-cut element to reduce the insertion loss of the intracavity element, which can theoretically achieve a linewidth of 1.3 kHz and a Stokes optical power output of up to 80% optical conversion efficiency. It is worth noting that as the fundamental linewidth is further reduced, the technical noise of the system will be the major obstacle restricting the realization of the fundamental linewidth in free-space-running BLs. Fortunately, the corresponding frequency stabilization or noise suppression techniques will help solve this problem. This study will provide a new technical route to achieve high-power, high-efficiency ultra-narrow linewidth laser radiation at special wavelengths.

Acknowledgements

This work was supported by the National Natural Science Foundation of China (No. 61927815), the Natural Science Foundation of Tianjin City (Nos. 22JCYBJC01100 and 20JCZDJC00430), the Shijiazhuang Overseas Talents Introduction Project (No. 20230004), the Program of State Key Laboratory of Quantum Optics and Quantum Optics Devices (No. KF202201) and Funds for Basic Scientific Research of Hebei University of Technology (No. JBKYTD2201).

D.J. acknowledges the support from the Postgraduate Innovation Ability Training Program of Hebei Province (No. CXZZBS2021030). R.P.M. acknowledges the support from

the Asian Office of Aerospace Research and Development (AOARD).

References

- J. Aasi, B. Abbott, R. Abbott, T. Abbott, M. Abernathy, K. Ackley, C. Adams, T. Adams, P. Adesso, and R. Adhikari, *Class. Quantum Gravity* **32**, 074001 (2015).
- S. Wehner, D. Elkouss, and R. Hanson, *Science* **362**, eaam9288 (2018).
- M. Endres, H. Bernien, A. Keesling, H. Levine, E. R. Anschuetz, A. Krajenbrink, C. Senko, V. Vuletic, M. Greiner, and M. D. Lukin, *Science* **354**, 1024 (2016).
- M. Li, X. Yang, Y. Sun, H. Jiang, R. P. Mildren, O. Kitzler, D. J. Spence, and Y. Feng, *Opt. Express* **31**, 8622 (2023).
- Y. Wang, C. Cui, Z. Lu, Z. Bai, Y. Wang, and H. Yuan, *Opt. Express* **30**, 35792 (2022).
- R. Fan, Z. Liu, D. Jin, T. Luo, N. Li, S. Li, Y. Wang, Y. Xia, and Z. Lu, *Opt. Express* **31**, 1878 (2023).
- X. Cheng, Z. Lin, X. Yang, S. Cui, X. Zeng, H. Jiang, and Y. Feng, *High Power Laser Sci. Eng.* **10**, e3 (2022).
- W. Liu, J. Song, P. Ma, H. Xiao, and P. Zhou, *Photonics Res.* **9**, 424 (2021).
- Y. Wei, W. Peng, J. Li, P. Jin, J. Su, H. Lu, and K. Peng, *Opt. Lett.* **48**, 676 (2023).
- Y. Guo, M. Xu, W. Peng, J. Su, H. Lu, and K. Peng, *Opt. Lett.* **43**, 6017 (2018).
- C. Robin, I. Dajani, and B. Pulford, *Opt. Lett.* **39**, 666 (2014).
- X. Yang, O. Kitzler, D. J. Spence, Z. Bai, Y. Feng, and R. P. Mildren, *Opt. Lett.* **45**, 1898 (2020).
- M. Merklein, I. V. Kabakova, A. Zarifi, and B. J. Eggleton, *Appl. Phys. Rev.* **9**, 041306 (2022).
- B. J. Eggleton, B. Luther-Davies, and K. Richardson, *Nat. Photonics* **5**, 141 (2011).
- B. J. Eggleton, C. G. Poulton, P. T. Rakich, M. J. Steel, and G. Bahl, *Nat. Photonics* **13**, 664 (2019).
- M. Merklein, I. V. Kabakova, T. F. Buttner, D. Y. Choi, B. Luther-Davies, S. J. Madden, and B. J. Eggleton, *Nat. Commun.* **6**, 6396 (2015).
- M. Garrett, Y. Liu, M. Merklein, D.-Y. Choi, K. Yan, S. J. Madden, and B. J. Eggleton, *J. Lightwave Technol.* **40**, 1672 (2022).
- C. K. Lai, D. Y. Choi, N. J. Athanasios, K. Yan, W. Y. Chong, S. Debbarma, H. Ahmad, B. J. Eggleton, M. Merklein, and S. J. Madden, *Adv. Funct. Mater.* **32**, 2105230 (2022).
- M. Merklein, B. Stiller, and B. J. Eggleton, *J. Opt.* **20**, 083003 (2018).
- Y. Qin, S. Ding, M. Zhang, Y. Wang, Q. Shi, Z. Li, J. Wen, and X. Jiang, *Opt. Lett.* **47**, 1638 (2022).
- S. Gundavarapu, G. M. Brodник, M. Puckett, T. Huffman, D. Bose, R. Behunin, J. Wu, T. Qiu, C. Pinho, N. Chauhan, J. Nohava, P. T. Rakich, K. D. Nelson, M. Salit, and D. J. Blumenthal, *Nat. Photonics* **13**, 60 (2018).
- Y. Tao, M. Jiang, L. Liu, C. Li, P. Zhou, and A. Z. Jiang, *J. Lightwave Technol.* **41**, 678 (2022).
- C. Shi, Q. Sheng, S. Fu, S. Sun, J. Zhang, W. Shi, and J. Yao, *Opt. Express* **28**, 2948 (2020).
- N. Chauhan, A. Isichenko, K. Liu, J. Wang, Q. Zhao, R. O. Behunin, P. T. Rakich, A. M. Jayich, C. Fertig, C. W. Hoyt, and D. J. Blumenthal, *Nat. Commun.* **12**, 4685 (2021).
- N. T. Otterstrom, R. O. Behunin, E. A. Kittlaus, Z. Wang, and P. T. Rakich, *Science* **360**, 1113 (2018).
- A. Debut, S. Randoux, and J. Zemmouri, *Phys. Rev. A* **62**, 023803 (2000).
- Y. Tao, M. Jiang, L. Liu, C. Li, P. Zhou, and Z. Jiang, *Opt. Lett.* **47**, 1742 (2022).
- T. Heupel, M. Weitz, S. Chu, and T. Hänsch, *Opt. Commun.* **140**, 281 (1997).
- D. Jin, Z. Bai, Z. Lu, R. Fan, Z. Zhao, X. Yang, Y. Wang, and R. P. Mildren, *Opt. Lett.* **47**, 5360 (2022).
- Z. Bai, R. J. Williams, O. Kitzler, S. Sarang, D. J. Spence, Y. Wang, Z. Lu, and R. P. Mildren, *APL Photonics* **5**, 031301 (2020).
- R. Barger, M. Sorem, and J. Hall, *Appl. Phys. Lett.* **22**, 573 (1973).
- K. Liu, N. Chauhan, J. Wang, A. Isichenko, G. M. Brodник, P. A. Morton, R. O. Behunin, S. B. Papp, and D. J. Blumenthal, *Optica* **9**, 770 (2022).
- M. W. Puckett, K. Liu, N. Chauhan, Q. Zhao, N. Jin, H. Cheng, J. Wu, R. O. Behunin, P. T. Rakich, K. D. Nelson, and D. J. Blumenthal, *Nat. Commun.* **12**, 934 (2021).
- O. Svelto and D. C. Hanna, *Principles of Lasers* (Springer, New York, NY, 2010).
- Z. Q. Yuan, H. M. Wang, L. E. Wu, M. D. Gao, and K. Vahala, *Optica* **7**, 1150 (2020).
- I. S. Grudin, A. B. Matsko, and L. Maleki, *Phys. Rev. Lett.* **102**, 043902 (2009).
- L. Jiang, L. Hansuek, C. Tong, and K. J. Vahala, *Opt. Express* **20**, 20170 (2012).
- H. Lee, T. Chen, J. Li, K. Y. Yang, S. Jeon, O. Painter, and K. J. Vahala, *Nat. Photonics* **6**, 369 (2012).
- S. Huang, T. Zhu, Z. Cao, M. Liu, M. Deng, J. Liu, and X. Li, *IEEE Photonics Technol. Lett.* **28**, 759 (2016).
- L. Richter, H. Mandelberg, M. Kruger, and P. McGrath, *IEEE J. Quantum Electron.* **22**, 2070 (1986).
- Z. Zhao, Z. Bai, D. Jin, Y. Qi, J. Ding, B. Yan, Y. Wang, Z. Lu, and R. P. Mildren, *Opt. Express* **30**, 30600 (2022).
- L. B. Mercer, *J. Lightwave Technol.* **9**, 485 (1991).
- G. Di Domenico, S. Schilt, and P. Thomann, *Appl. Opt.* **49**, 4801 (2010).
- I. V. Kabakova, R. Pant, D. Y. Choi, S. Debbarma, B. Luther-Davies, S. J. Madden, and B. J. Eggleton, *Opt. Lett.* **38**, 3208 (2013).
- R. Pant, E. Li, D. Y. Choi, C. G. Poulton, S. J. Madden, B. Luther-Davies, and B. J. Eggleton, *Opt. Lett.* **36**, 3687 (2011).
- K. Hu, I. V. Kabakova, T. F. Buttner, S. Lefrancois, D. D. Hudson, S. He, and B. J. Eggleton, *Opt. Lett.* **39**, 4651 (2014).
- J. H. Geng, S. Staines, Z. L. Wang, J. Zong, M. Blake, and S. B. Jiang, *IEEE Photonics Technol. Lett.* **18**, 1813 (2006).
- D. Jin, Z. Bai, M. Li, X. Yang, Y. Wang, R. P. Mildren, and Z. Lu, *Opt. Express* **31**, 2942 (2023).
- H. Lee, M. G. Suh, T. Chen, J. Li, S. A. Diddams, and K. J. Vahala, *Nat. Commun.* **4**, 2468 (2013).